RESEARCH ARTICLE

Quantifying Marine Oil Slick using the Hydrocarbon Spectra Slope Index (HYSS): A Case Study of the 2010 Deep-water Horizon Spill in the Gulf of Mexico

Kamorudeen. Tunde Olagunju [1,*], Callen. Scott Allen[2], Samuel. Bamidele Olobaniyi[1] , Kayode. Festus Oyedele[1]

[1] Department of Geosciences, University of Lagos, Lagos, Nigeria.

[2] Department of Geography, University of Mary Washington, Fredericksburg, VA, USA**.**

* Corresponding author : kolagunju@unilag.edu.ng.
Tel.:+234-803-716-8057

Abstract

Mapping the extent and quantifying oil slick in ocean spills is one of the major objectives for monitoring and clean-up programs. Hyperspectral sensors are among the few remote sensing tools with potential for quantifying hydrocarbon oil on water and on other background substrates. At present, methods used to process hyperspectral data for quantifying hydrocarbon oil relies on delineating shapes and wavelength position of key diagnostic features within shortwave infrared (SWIR), particularly at 1.73μm and 2.30μm, which are often affected by the spectral features from the background substrates. Rather than the shape, the absorption maxima of hydrocarbon diagnostic features has shown potential for quantifying oil slick abundance classes via the Hydrocarbon Spectral Slope index (HYSS). In this research, the discriminative power of HYSS index for quantifying ocean oil slick is demonstrated, using Advance Visible and Infrared Imaging Spectrometer (AVIRIS) data from the 2010 Deep-water Horizon (DHW) spill from the Macondo well-head in the Gulf of Mexico. The results suggest good discrimination of oil and water as well as quantification of the oil slick into different oil abundance classes, representing different oil-water ratio and/or thickness. The validation of HYSS results shows good agreement with visual records of the spill within the image scene. Five oil abundance classes were discernible from studied AVIRIS scenes. These results were obtained empirically, without site-specific reference spectra, suggestive of a potential index for rapid broad area search. Change detection statistics of oil coverage at three separate intersects (ITT 1, ITT 2, and ITT 3) with before and after image coverage show reduced oil coverage percentages of 70%, 11.5%, and 0% respectively. These percentage reductions are in agreement with visual display of oil coverage as affected by dispersion induced by ocean currents and chemical dispersant application within the respective time lags of these image data acquisition.

Keywords: Hydrocarbon oil, Hyperspectral, Optical remote sensing, AVIRIS, Oil spill, Deep-water Horizon, HYSS

1. Introduction

An estimated 2.9 million metric tons of hydrocarbon oil was spilled in the world oceans between 1980 to 1989 while an additional 600,000 metric tons are estimated as yearly contribution from seepages from around the world (Kvenvolden and Cooper 2003, Etkin 2001) This pollution trend is increasing across the globe especially with recent net increases in oil production (Li et al. 2016). Oceanic oil spills across the globe result from human activities such as oil exploration and transportation (National Research Council 2003, Leacock 2005). Fresh and weathered oils have devastating effects on the marine ecosystem and human life (Tatem, Cox, and Anderson 1978, Obida et al. 2018, Liu et al. 2016, Waldichuk 1974). Quantifying oil slick abundance during and after spill events is vital for oil spill monitoring and clean-up programs (Fritt-Rasmussen et al. 2012, Shi et al. 2016, Fritt-Rasmussen and Brandvik 2011, Sarbatly, Krishnaiah, and Kamin 2016, Bullock et al. 2017). Consequently, attempts to detect and quantify hydrocarbon oils in the ocean has been given significant attention in previous work (Clark et al. 2010, Lu, Zhan, and Hu 2016,

Scafutto and Souza Filho 2016). Hyperspectral imaging offers potential to quantify and characterize hydrocarbons even on different background substrates, including water (Clark et al. 2010, Lammoglia and Filho 2011, Lammoglia and Filho 2012, Lammoglia and Souza Filho 2012a, Asadzadeh and de Souza Filho 2016, Kühn, Oppermann, and Hörig 2004b, Wettle et al. 2009, Allen and Krekeler 2010, Estes and Senger 1971, Fingas and Brown 2017). Hydrocarbon oil exhibits diagnostic spectral signatures in the short wave infrared region (SWIR); particularly around 1.20μm, 1.73μm, and 2.30μm wavelength positions (Clark et al. 2010, Kühn, Oppermann, and Hörig 2004a, Andreoli et al. 2007). These absorption features correspond to overtones and combination bands common in hydrocarbons, which has been proved useful for discriminating and quantifying oil slicks types and against different backgrounds (Clark et al. 2010, Lammoglia and Filho 2011, Kühn, Oppermann, and Hörig 2004b, Scafutto and Souza Filho 2016). The shapes and wavelength position of these key hydrocarbon features are significant parameters that provides quantitative information on hydrocarbon oil. Presently, there are multiple methods for

extracting relevant information for quantitative analysis of hydrocarbon on hyperspectral data including chemometrics, artificial neural networks, and other similar statistical models (Lammoglia and Filho 2011, Lammoglia and Souza Filho 2012b, Lammoglia and Filho 2015, Clark et al. 2010). These data analysis techniques rely on shapes of diagnostic absorption features. Therefore, error in delineating these parameters may lead to inadequate data or misleading interpretations. This is a feasible due to the complex chemistry of hydrocarbons, especially crude oil, and is further complicated when background substrates interference with the hydrocarbon spectral features. In contrast, the HYSS index uses absorption depth maxima of the most persistent diagnostic absorption features, with proven potential for characterizing and quantifying hydrocarbon oil (Olagunju et al., 2023). In this study, we aim to investigate the capability of hydrocarbon spectra slope model (HYSS) for quantitative evaluation of hydrocarbon oil, using hyperspectral data of marine oil slicks.

In this study, we quantified the floating oil slick from the Deep-water Horizon event on AVIRIS data using oil-water ratios and oil thickness as a proxy to measure relative oil abundance. HYSS index is a spectral ratio of reflectance and wavelengths at absorption maxima of key hydrocarbon oil diagnostic features at 1.73µm and 2.30µm (Olagunju et al., 2023). Oil-water ratios with higher oil content often have higher reflectance than those with less oil, which tend to have very low reflectance (Clark et al. 2010). Previous authors have determined that the absorption features at 1.73µm and 2.30µm are persistent against interfering effects from most background substrates (Scafutto and Souza Filho 2016, Kühn, Oppermann, and Hörig 2004a, Clark et al. 2010). A slope formed between these points provides a quantification and characterisation of different classes of oil abundance due to difference in oil-water ratios and thickness (Olagunju et al., 2023). Oil slick emulsion often occurs in different oil-water ratios, due to the mixing effect of the ocean current (Svejkovsky et al. 2016, Svejkovsky and Muskat 2006, Lammoglia and Filho 2011). HYSS resolves higher oil-water ratios and thicker oil as a steeper slope than lower ratios and less thick oil, which tend to have a more gentle slope. In the case of clean water, a slope approaching zero is common since reflectance values at both points is similar due to water's strong absorption in the SWIR. Therefore, a slope value is a measure of relative oil abundance both in term of oil-water ratio and oil thickness. This study demonstrates the quantification of relative oil abundance, using the data of the Deep-water Horizon (DWH) spill in the Gulf of Mexico in 2010.

The DWH spill remains the largest marine spill in history and it is only ranked second to the Kuwait-Iraq war (onshore) spill as the largest recorded spill in the world history (Leacock 2005, Murphy et al. 2016, Fingas 2016). DWH is also the most studied of all spill events (Murphy et al. 2016) with a large archive of hyperspectral data. This spill lasted eighty-seven (87) days, provided ample opportunity to produce a large marine spill footprint and oil emulsions with a variety of different oil-water ratios and varying thicknesses (Svejkovsky et al. 2016, Sun et al. 2016, Clark et al. 2010). Advanced Visible and InfraRed Imaging Spectrometer (AVIRIS) was flown over the DWH spill; data acquired on May 17, 2010 covered a significant part of the spill with limited cloud cover. These data include lines 8 to 14 as shown in figure 1 below. After pre-processing, HYSS index was applied to this dataset, which provide new insights into the quantification of the oil slick and also

reveal a potential for the use of these methods as tool for rapid response in ocean spill management. Furthermore, as a simple normalized index, HYSS requires very little computational time and minimal spectral channels for oil slick quantification (Olagunju et al, 2023).

2. Data, Materials and Methods

2.1 Dataset

The AVIRIS data portal from United States Geological Survey (USGS) hosts all AVIRIS data flown from 2006. We used flight lines 08 to 14 over the DWH spill for this case study. Some of these flight lines (Runs 10, 11, and 14) cover the core of the spill on May 17, 2010, with limited cloud cover (see figure 1 below). Data from Moderate Resolution Imaging Spectrometer (MODIS) is displayed in the background in this figure, overlaid by the AVIRIS flight lines. The AVIRIS flight lines are already orthorectified, therefore, the only pre-processing was converting the data from radiance to reflectance (section 4.1). We then applied the HYSS index to the data. The summary of the theory of HYSS is explained in section 3.0 while the reader is referred to Olagunju et al 2023 for details.
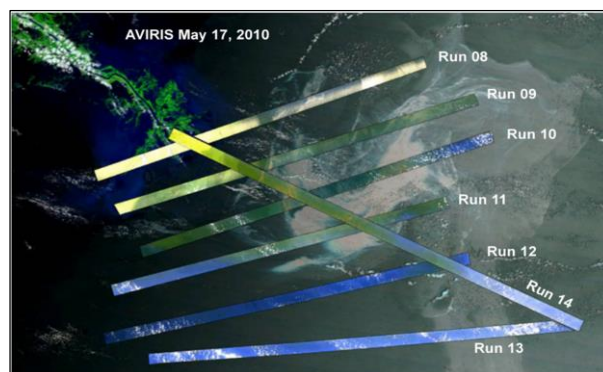

Fig 1. AVIRIS flight lines (Line 8 – 14) acquired on 17th of May, 2010 over the core of the Deepwater Horizon Spill in the Gulf of Mexico. The background image is the MODIS data from the same day (Clark et al., 2010).

2.2 Pre-processing

As mentioned above, AVIRIS data are available already orthorectified from the AVIRIS data portal. Generally, we explore data and metadata to check for possible gross error. Afterward, we used the Fast Line-of-sight Atmospheric Analysis for Hypercube data (FLAASH) algorithm to remove the atmospheric contribution and convert the data from radiance to reflectance for all flight lines (Kaufman et al. 1997). The estimated water vapour and scene-average visibility within the flight scenes range between 2.64cm to 3.67cm and 26.4km to 62.1km, respectively. Subsequently, these data were checked for bad bands due to system noise and water absorption features. The range of bad bands observed across all image scenes are within bands 57- 69 (899.72nm – 1005.56nm); bands 79 – 87 (1101.52nm – 1177.92nm); bands 102 – 121 (1303.23nm – 1492.65nm); bands 149 – 177 (1771.63nm – 2027.57nm); and bands 215 – 224 (2406.88nm – 2496.23nm). These ranges of bad bands were removed manually, by reviewing the data for the typical abnormalities in the common target spectra due to lingering atmospheric absorption/scattering and low signal to noise ratios. The target features used for this purpose are; cloud, water surface, dark areas (area of little or no illumination), vegetation, land (where available) and the surface oil at varying illumination conditions.

Therefore, the product of this pre-processing stage is a reflectance image of each flight line with bad bands removed. Note that the removed bands are not close (i.e., within 40 nm) to any hydrocarbon bands and those used in HYSS index.

2.3 Hydrocarbon Slope Map

Hydrocarbon Spectra Slope (HYSS) index is the ratio of the difference in reflectance of the absorption maxima depth of key hydrocarbon bands to the difference in their corresponding wavelength intervals (Olagunju et al, 2023). In other words, the slope value measures the absorption depth of these hydrocarbon spectral features, which changes with oil-water ratio and thickness, hence, it can serve as a proxy for measuring relative oil abundance. Equation 1 represents the mathematical expression for HYSS, which was computed for each image pixel from the AVIRIS runs. Scene areas with high oil abundance (oil-water ratio with higher oil content/thickness) have higher reflectance, hence, resolved as relatively steep slopes (i.e., -0.70 to -0.30) while the areas with low oil abundance produced low values to the gentle slope (i.e., -0.10 to -0.02) between 1.73µm and 2.30µm. In the case of clean water pixel, very low or no slope indication is expected (i.e., -0.02 to -0.00) as reflectance at the two spectral channels used is similar due to water's strong absorption in the SWIR.

$$S \ = \ \frac{a-b}{c-d} \quad (1)$$

Where a = Reflectance at 2.30µm; b = Reflectance at 1.73µm; c = Wavelength value of b (2.30µm); d = Wavelength value of a (1.73µm).

The slope map for each flight line was created by applying the HYSS equation on the corrected reflectance images using band math. In figure 2, the slope maps are shown along with their true colour image composite for visual comparison. Flight lines 10, 11, and 14 captured the spill centre with substantial amounts of oil across different oil abundance classes. In contrast, flight line 12 covers areas with little or no oil slick as shown in this figure. These slope maps in figure 2 and their corresponding true colour images are shown at same spatial extent and the slope maps are scaled the same for comparison purposes. Five distinct oil abundance classes were established with unsupervised classification and they are subjectively denoted with different colours as very high, high, moderate, low, and low very oil abundance classes (see figure 2's legend). The ocean water is depicted in white as the background substrate on displayed on slope map as shown in figure 2 and figure 4 (section 2.4).
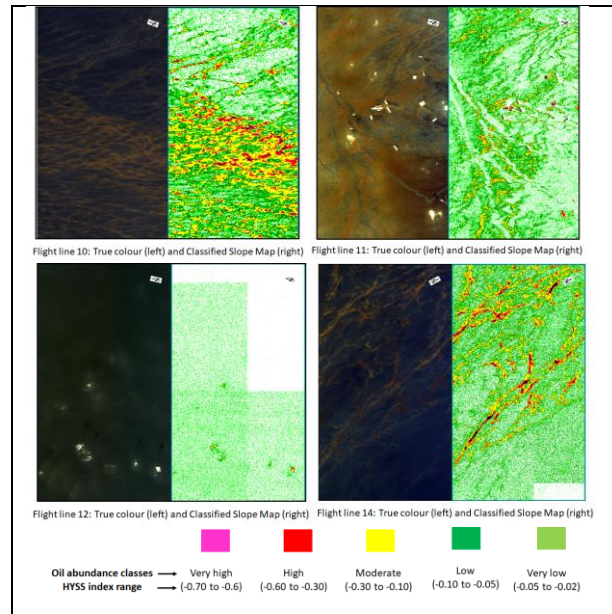

Fig 2: Slope map of Deep-Water Horizon spill across flight lines 10, 11, 12, and 14 (along with true colour image at same spatial extent), depicting distribution of varying classes of oil abundance with colour schemes against ocean water (white). In agreement with figure 1, Flight lines 10, 11, and 14 contain substantial oil slicks whereas flight line 12, which is far from spill core, does not. Loss of textural information at the top and bottom left of the image 12 and 14 is due to poor mosaic of the raw images.
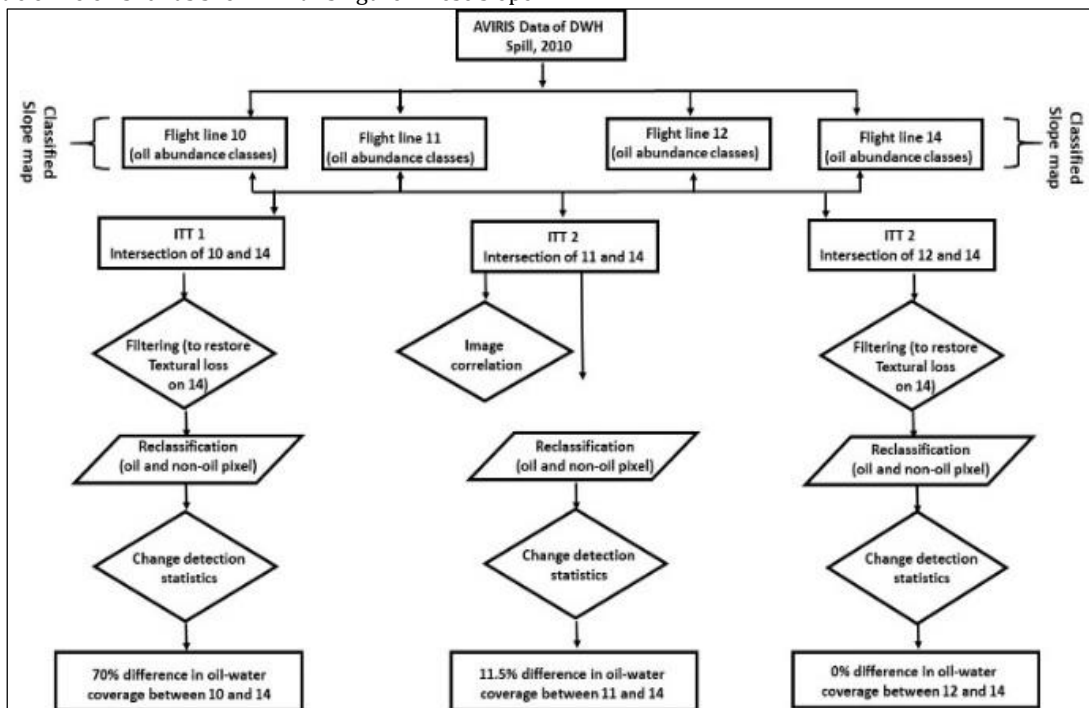

Fig 3. Flow chart showing the procedure for validation of slope map

Table 1: Comparison of class boundary and percentage coverage of different oil abundance on classified slope map on intersection images from flight line 14 with flight lines 10, 11, and 12.

Class Name	Range and percentage of Slope Value Across Class Boundaries/Oil Abundant Classes													
	Cloud/Shadow		Very High		High		Moderate		Low		Very Low		water	
Flight line/ acquisition time	Slope Range	% scene coverage	Slope Range	% scene coverage	Slope Range	% scene coverage	Slope Range	% scene coverage	Slope Range	% scene coverage	Slope Range	% scene coverage	Slope Range	% scene coverage
10 19:54:57-20:27:31	-2.2	0.05	-0.70	0.04	-0.60	0.67	-0.30	5.12	-0.10	9.33	-0.05	20.64	-0.02	64.13
	to	0.02	to	0.01	to	0.10	to	0.56	to	2.87	to	11.21	to	89.21
14 22:11:56 – 22:45:32	-0.70		-0.60		-0.30		-0.10		-0.05		-0.02		0.23	
11 20:32:39 – 20:57:46	-4.86	0.10	-0.70	0.03	-0.60	0.35	-0.30	3.24	-0.10	8.44	-0.05	20.52	-0.02	67.25
to		0.23	to	0.08	to	0.73	to	4.24	To	12.93	to	19.58	to	62.11
14 22:11:56 – 22:45:32	-0.7		-0.60		-0.30		-0.10		-0.05		-0.02		0.29	
12 21:01:43-21:36:37	-2.75	0.00	-0.70	0.00	-0.60	0.00	-0.30	0.00	-0.10	0.05	-0.05	6.37	-0.02	93.58
to		0.00	to	0.00	to	0.00	to	0.00	to	0.04	to	8.33	to	91.62
14 22:11:56 – 22:45:32	-0.70		-0.60		-0.30		-0.10		-0.05		-0.02		0.26	

2.4 Validation of AVIRIS Slope Map

The flow chart in figure 3 shows the procedure adopted for validation of the slope map. Validation of the results of the HYSS index is important in order to measure the accuracy of oil slick quantification achieved on the slope map across the AVIRIS flight lines. The image of DWH spill in Figure 1 shows the flight lines of AVIRIS data, numbered in sequence of acquisition. Seven flight lines (8-14) cover the spill as shown in the said figure. However, three flight lines (10, 11, 14) covers the core of the spill and are therefore used in the validation analysis. Flight line 12 is also included in the validation analysis as this flight line slightly covered only oil sheen and largely the ocean water. The time lag between successive flight line is roughly about 30 minutes. In other words, the cross-cutting flight line 14 has an acquisition time successively closer to flight line 12, 11, and 10.
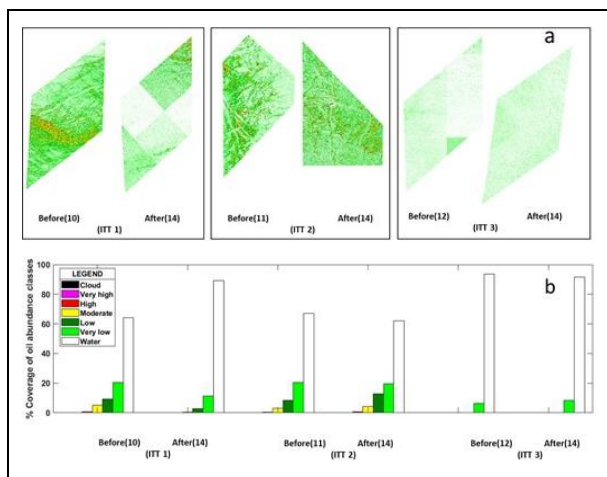

Figure 4: Slope map at intersection of flight-line 14 and other crosscutting flight lines (10, 11, and 12) showing variation of percentage coverage of oil abundance classes at the three intersections (a). Below intersection images is the bar chart, showing percentage coverage different relative oil abundance classes (b)

First column of Table 1 above shows the time lag between each flight line. In an attempt to validate the capability of the HYSS for discriminating oil abundance classes from the background ocean water, we computed HYSS in order to determine oil occurrence/coverage at each intersection of flight line 14 and the other flight lines (figure 4a). Tabular results are in table 1 and depicted as a bar chart in figure 4b. However, with a dynamic ocean current and ongoing impacts from chemical dispersant, significant change is expected at each intersection due to time-lag of approximately 70 (lines 12 and 14) to 140 (lines 10 and 14) minutes (Svejkovsky et al. 2016, Sun et al. 2016). With these two drawbacks, class to class comparison of oil abundance on before (flight line 10, 11, and 12) and after image (flight line 14) is not possible. In the three intersections shown in figure 4, the before and after images for flight lines 11 and 14, respectively, reveal similar oil slick ocean coverage. We used correlation of each pixel in the before image to each pixel in the after image to assess the degree of variance at this intersection. However, image correlation reveals a very low correlation coefficient of 0.16, suggesting substantial redistribution of the oil slick within the time lag of acquisition of both images, which we discuss further in sections 2.5 and 2.6 below. This is not surprising because image correlation does not depict the coexistence of quantity of oil coverage averaged across the whole image, but rather, compares the oil abundance classes at the same pixel-pixel locations on both images, which is expected to be strongly influenced by ocean current dynamism and the effect of dispersant over the time lag. While the HYSS slope map was intended to assess accuracy of mapping oil abundance classes, the substantial change between flight lines limited the utility to oil slick-sea water discrimination (section 2.5). To achieve this comparison, a subset of flight line 14 and the corresponding preceding flight lines at each intersection were extracted and classified, as shown in figure 5. These classified images were further pre-processed for change detection statistics as discussed in section 2.5.

HYSS index measures relative oil abundance, therefore, the class boundaries are subjective due to the effect of internal and external factors relating to the image scene. Possible internal factors are pixel mixing, sensor/platform noise, and calibration while the external factors may include scene illumination, viewing geometry, and sun glint (Clark et al, 2010). A slight variation observed in the range of slope values to their corresponding oil abundance classes across all flight line (as shown in table 1) is attributable to these factors and the occurrence of natural and artificial objects in the scene such as ships, clouds, and shadow. Variation of slope value is only visible on the upper and the

lower bound in first and last class boundary as shown in table 1. That is, cloud and shadow have class boundaries with a varying slope values (i.e., -2.2 to -0.7 for flight line 10, -4.86 to -0.7 for flight line 11 and -2.75 to -0.7 for flight line 12). Similarly, varying lower class boundary occurred for the three flight lines (i.e., -0.02 to 0.23 for flight line 10, -0.02 to 0.29 for flight line 11 and -0.02 – 0.26 for flight line 12). The variation of slope value is highest on flight line 11 image because of the presence of spill combating ship within this mage scene.

To validation slope map via change detection of oil slick coverage comparison on intersection images (i.e., oil slick-seawater discrimination), we used change detection statistics. This comprises of evaluation and comparison of quantity of oil and non-oil pixel on corresponding subsets at each intersection. Image correlation did not work so well for the validation of slope map. Not only because of the expected mixing and redistribution of oil slick due to dynamism of ocean current and the use of dispersant within the time lag between the corresponding flight line, but correlation also checks for location accuracy for all oil abundance classes represented by varying slope values on both raster images of each intersection. Change detection statistics is therefore considered for a validation of oil presence and coverage at the three intersects. This option is more appropriate, since it provides percentage changes of oil and non-oil pixel at each intersect within the time lag of line 14 and other flight lines with agreement to visual changes resulting from redistribution of oil slick by ocean current and the effect of dispersant.

2.5 Change detection on oil slick-and seawater discrimination

The slope maps are raster images of the flight lines, with pixel values representing the HYSS value, as a measure of oil abundance classes as shown in figure 2 and figure 4. Five mainly oil classes were distinguished on AVIRIS flight lines as discussed in section 2.4 above. However, change detection is intended to assess the accuracy of HYSS model in discriminating oil slick from seawater by comparing pixel values at same location on before (flight line 10, 11, 12) and after (flight line 14) of DWH spill images scene. To assess the changes between slope values, oil and non-oil pixels in these images, we used change detection statistics. As earlier discuss in section 2.4, two drawbacks do not allow distinct comparison of pixel-to-pixel slope value based on oil abundance classes. 1) Significant change in distribution of oil coverage and oil abundance classes due to dynamic ocean current and 2) the effect of the dispersant used to combat the spill as reported in previous works (Svejkovsky et al. 2016, Clark et al. 2010). These two drawbacks are expected to hindered pixel to pixel slope value comparison at each intersect for validation of oil abundance classes. For instance, pixel-to-pixel slope value comparison was carried out to check correlation of pixel-to-pixel slope value at intersection of 11 and 14 flight line, where least change was observed. The result is a very low value of 0.16 correlation coefficient. Unlike image correlation analysis, change detection statistics of before and after image of spill scenes is meant to assess changes of oil and non-oil pixel, at the three intersections for comparison. Intersections used for validation procedure are 10/14 intersection (intersect 1: ITT1), 11/14 intersection (intersect 2: ITT2) and 12/14 intersection (intersect 3: ITT3). These intersections were chosen based on the time lag of other flight lines relative to crosscutting flight line 14 and the presence of oil slick at each intersection, as depicted on figure1 and figure 4. The background MODIS image showed a relative abundance of

oil on ocean (as grey shades) on the day of acquisition of the AVIRIS data (Clark et al. 2010). This image guided the selection of flight line covering the spill's core at intersection with flight line 14. Corresponding subset of slope map of the same extent (derived from flight light 10, 11, 12 and 14) are obtained at ITT1, ITT2 and ITT3. To prepare slope map of image scene at intersections for image correlation and change detection statistics, cloud, ships and shadow were digitized and masked out of the subset images, using true colour composite of each AVIRIS flight lines as guide. The exclusion by masking is intended to limit erroneous value on images, caused by these objects which may affect the result of change detection statistics. In general, cloud, ship and shadow give close but slightly higher slope value to oil. These values may be mistaken to oil, especially when affected by other internal/external factors (see section 2.4 above). Procedure adopted for image correlation and change detection statistics were discussed below.

For the correlation analysis, the corresponding subset images at intersect were used to create a shapefiles to segregated oil pixel from ocean water pixel. These shapefiles were subsequently used to expunge the non-oil pixel (mainly water pixel) from the subset images. The subset images, containing only oil pixel slope value, are then layer stalked for correlation analyses. This analysis was carried out only for ITT2 as this intersect has high chance of success for correlation since substantial amount of oil was observed here and the time lag between these successive images is the shortest for scene with oil slick. The correlation coefficient obtained is low (0.16) as expected because, even though oil occurrence was obvious on both corresponding images. Oil abundance classes cannot stay the same over the time lag between the two images, not only for the dynamic nature of the ocean current but also due to the effect of dispersant that was reported to be in use within the timeframe of the image acquisition. For this reason, correlation analysis was not carried for ITT1 and ITT3 for the longer time lag and insignificant oil coverage respectively and cannot be used for validation of slope map.

For change detection statistics, subset from flight line 10, 11 and 12 were used as initial stage while subset from flight line 14 was used as final stage at the three chosen intersections as shown in figure 3. In this study, two classification method were used to obtain oil abundance classes of oil slick on slope map, i.e., density slicing and Isodata classification. Density slicing of the slope map was performed, virtually guided by the true colour composite of AVIRIS image of the spill. Both methods gave similar result with five oil abundance classes (figure 2 and 4). For change detection, we used unsupervised isodata classification since no training parameter is available to describe the spill. That is, the classification is based on image statistics, using minimum distance techniques for pixel clustering (Richards and Richards 1999). The Isodata parameter for classification are chosen, to obtain optima classification, as depicted on the slope maps. Chosen Isodata parameters use are 13 maximum iteration, with 1% change threshold (Tou and Gonzalez 1974). To reduce the noise in the classified map, smoothing was applied using 3 x 3 pixels kernel size with aggregate minimum size of 30 pixels. These parameters are maintained for all subsets, to enable comparison between corresponding subsets and intersections for change detection statistics. The masked subsets images as described above (for correlation analysis) were reclassified as oil and non-oil (water) pixel, by merging all oil abundance classes as oil pixel. After classification, Kuan filtering was used to restore textural

loss in the image, which is inherent on flight line 14 as shown in figure 2 and 4. This filter replace the original pixel with calculated pixels based on local statistics (Zhenghao Shi and Ko B. Fung 1994). The filtering was basically used on subset image at these intersections, with textural loss (i.e., ITT1 and ITT3). The loss in textural information is thought to be as a result of the mosaic effect on this images or acquisition error. Illustrations of this occurrence is shown at top right and bottom right of the slope map of flight line 12 and 14, 10 and 14 (respectively) in figure 2. Before the application of the filter on flight line 14 at ITT1

and ITT3, this image subsets were segmented into sub-image with coherent textural pattern. Each image segment were separately filtered before they are merged for classification, in order to enhance the filtering process. Filtering procedure and subsequent reclassification of subset images by merging all oil abundance class as oil pixel and water pixel as non-oil pixel produced oil coverage map for the three intersection images. Figure 5 shows oil coverage on subset images at the three intersection while Table 2 shows the result of the change detection statistics for each intersection.

Table 2: Change Detection Statistics for the Validated Intersections at Deep-water Horizon Spill based on Hydrocarbon Spectra Slope Index

Intersection	Classification for Change Detection (Percentage %)	Initial state (Flight line 10 intersect image)			
		Acquisition timeframe: 19:54:57 – 20:27:31			
		Oil	Water	Total Row	Class Total
	Unclassified	0.006	0.161	0.085	100
	Oil	15.477	14.028	99.982	100
	Water	84.517	85.811	99.919	100
ITT 1: 10/14	Class Total	100	100		
	Class Changes	84.523	14.189		
	Image Difference	-70.198	68.742		
		Initial state (Flight line 11 intersect image)			
		Acquisition timeframe: 20:32:39 – 20:57:46			
	Unclassified	0.100	0.338	0.147	100
	Oil	55.539	52.646	97.798	100
	Water	44.051	46.792	98.574	100
	Cloud/Ship/Shadow	0.311	0.224	51.997	100
ITT 2: 11/14	Final state (Flight line 14 intersect image) Acquisition time: 22:11:56 – 22:45:32	Class Total	100	100	
		Class Changes	44.461	53.208	
		Image Difference	-11.597	23.563	
		Initial state (Flight line 12 intersect image)			
		Acquisition timeframe: 21:01:43 – 21:36:37			
	Unclassified	----	0.078	0.080	100
	Oil	----	0.236	100	100
	Water	----	99.686	99.995	100
	Class Total	----	100		
	Class Changes	----	0.314		
ITT 3: 12/14	Image Difference	----	-0.309		

2.6 Result of Validation exercise

The result of image correlation is obviously not useful for validation since the dispersion obviously would have resulted in redistribution of oil – water location as well as the location and quantities of oil abundance classes within the time lag of intersection images. This explained the low correlation coefficient of 0.16 obtained at ITT 2 intersection involving flight line 11 and 14 with shortest time lag of scene containing oil, as shown on table 1 and figure 4. The slope values generated by the HYSS index represents different oil abundance classes of which five main classes were resulted as shown on figure 2 and table 1. Oil slick dispersion due to the ocean current and the use of dispersant within the time-lag of the images does not favour image correlation as validation method, since this analysis checked for changes in pixel to pixel slope value and not only changes between oil abundance classes. Hence, the need for change detection statistic to compare oil quantity change on intersection images as a means of validating the slope map. To achieve this, all oil abundance classes were merge as oil pixel on the three intersection images.

Therefore, these images have only oil and water pixels as input for change detection statistics. Subset intersection images of 10, 11 and 12 flight line were used as initial state, while subset intersection images of flight line 14 were used as final images as shown in figure 5 and table 2 below.

The table 2 below shows the summary of the result of Change detection Statistics at the three intersections. Although, this analysis tool does not give location specific comparison of oil abundance classes as hoped attainable. However, it does provides the information of percentage changes that occurred between water and oil coverage on intersection images. This gives a relatively comparison of oil – water redistribution at each intersection within the recorded time-lag. Therefore, we can relate the result of the change detection statistics to the expected changes, while this analysis tool provides quantitative measure of these changes. At ITT 1, 84.5% of pixels that represented oil on flight line 10 has changes to water while only 14% of pixels that represented water on flight line 10 changed to oil on flight line 14 within the image time lag. This resulted in 70% overall change in oil – water coverage within this image time lag. Similarly at ITT 2, 55.5% of pixels that represented

oil on flight line 11 remained as oil while only 44% of pixels that represented oil on this flight line changed to water on flight line 14 within their respective time lag. Hence 11.5% overall change in oil-water coverage estimated. Also at ITT 3 where oil sheen are reported in previous works (Clark et al. 2010, Svejkovsky et al. 2016), 0% of oil was represented on flight line 12 and only 0.24% was recorded on flight line 14 within the image time lag, while little or no change is recorded in the percentage of oil-water coverage.
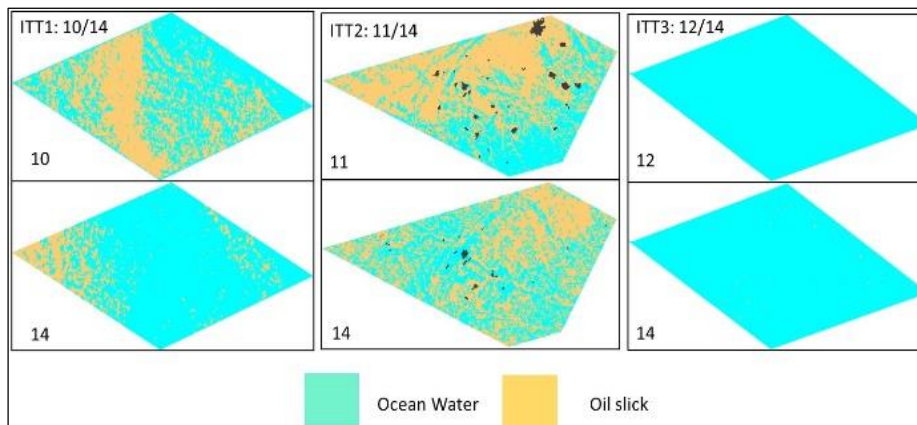
Fig 5: Showing change detection map for ITT 1, ITT 2 and ITT 3, using the slope map generated by HYSS index. Image 11 and 14 contained masked area of substantial cloud cover and spill combating ships (in black colour).

3.0 Discussion of Results

The slope map from HYSS has shown a good agreement with the results presented in previous work, both on discrimination and relative distribution of oil abundance classes based on oil – water ratio (Clark et al. 2010). Furthermore, though a relative measure, the oil abundance class discrimination revealed by this method is completely empirical and independent of site-specific reference spectra samples. Five distinct classes from (presumably) very thick oil to oil sheen were revealed as shown in figures 2 and 4. In addition, this method is computationally fast, which saves time and therefore can be useful for rapid broad area search, in addition to monitoring and assessment of spill sites. The primary discriminative power of HYSS index is the use of most persistent absorption features in the SWIR, specifically at 1.73μm and 2.30μm (Kühn, Oppermann, and Hörig 2004b, Hörig et al. 2001, Andreoli et al. 2007, Clark et al. 2010). These overtones and combination band are associated with the C-H stretching of alkane compound, which represents the major constituent of most hydrocarbon oils (Clark et al. 2009). These two absorption features are resilient, appear with minimal oil quantities (<1 g/cm2), and their wavelengths position are relatively stable in all hydrocarbon oil and also in spectral mixture with several background materials (Cloutis 1989, Kühn, Oppermann, and Hörig 2004b, Hörig et al. 2001, Andreoli et al. 2007, Clark et al. 2009, Correa Pabón and Souza Filho 2016, Scafutto and Souza Filho 2016, Allen and Krekeler 2010, Allen and Satterwhite 2006).

Some natural and artificial non-hydrocarbon materials are potential confusers. On the slope maps, vegetation, clouds, shadows, and ships respond to this ratio with slope values mimicking thick hydrocarbon oil (HYSS <-0.7) values. Therefore, occurrence of such objects and other similar objects in the scenes may affect the accuracy of hydrocarbon oil quantification. Scene content exploration for these non-oil objects is therefore important to minimize false positives. Furthermore, the effects of varying internal and external factors on HYSS values needs to be investigated. In this research, the observed range of slope values slightly varies within different flight lines. This variation may also be present within images in the same flight line, even if not significant. Careful observation of the true colour AVIRIS composite show marked variation in illumination due to varying sun angle and viewing geometry within flight lines. Therefore, further study on the possible effects of common internal and external image factors on slope values is merited. The validation exercise presented in the study left a knowledge gap due the limitation in the data used in this research. The time lag in the acquisition of each flight lines and the subsequent dispersion and redistribution of oil abundance classes by ocean currents and application of dispersant were limiting factors in this exercise.

4.0 Conclusion

The potential of HYSS index has been demonstrated for detection and quantification of hydrocarbon oils on ocean water, using hyperspectral data. This method uses a simple ratio technique involving two persistent absorption features which are also common to hydrocarbon oils, even in mixed spectra. The results show a good agreement on oil abundance classes and distribution pattern in the same dataset from previous studies. However, unlike previous works, this new method quantifies oil slicks using one dataset, completely empirical and independent of site-specific reference spectra. It is also computationally fast, which saves time and therefore can be useful for rapid broad area search. Further work is however needed to investigate internal and external image factors that may affect the HYSS values of hydrocarbon oil, such as illumination geometry, viewing geometry, sun angle, sun glints, signal to noise ratio, and the effect of the oils' bidirectional reflectance distribution functions (BRDF).

Acknowledgements

References

Allen, and Krekeler. 2010. "Reflectance spectra of crude oils and refined petroleum products on a variety of common substrates." Active and Passive Signatures.

Allen, C Scott, and Melvin B Satterwhite. 2006. "Reflectance spectra of three liquid hydrocarbons on a common

sand type." Algorithms and Technologies for Multispectral, Hyperspectral, and Ultraspectral Imagery XII.

Andreoli, G, B Bulgarelli, B Hosgood, and D Tarchi. 2007. "Hyperspectral analysis of oil and oil-impacted soils for remote sensing purposes." European Commission Joint Research Centre: Luxembourg:36.

Asadzadeh, Saeid, and Carlos Roberto de Souza Filho. 2016. "Investigating the capability of WorldView-3 superspectral data for direct hydrocarbon detection." Remote Sensing of Environment 173:162-173. doi: http://dx.doi.org/10.1016/j.rse.2015.11.030.

Bullock, Robin J., Srijan Aggarwal, Robert A. Perkins, and William Schnabel. 2017. "Scale-up considerations for surface collecting agent assisted in-situ burn crude oil spill response experiments in the Arctic: Laboratory to field-scale investigations." Journal of Environmental Management 190 (Supplement C):266-273. doi: https://doi.org/10.1016/j.jenvman.2016.12.044.

Clark, Roger N, John M Curchin, Todd M Hoefen, and Gregg A Swayze. 2009. "Reflectance spectroscopy of organic compounds: 1. Alkanes." Journal of Geophysical Research: Planets 114 (E3).

Clark, Roger N, Ira Leifer Gregg A. Swayze, K. Eric Livo, Raymond Kokaly, Todd Hoefen,, Michael Eastwood Sarah Lundeen, Robert O. Green, Neil Pearson, Charles Sarture, Ian McCubbin,, and Eliza Bradley Dar Roberts, Denis Steele, Thomas Ryan, Roseanne Dominguez. 2010. "A Method for Quantitative Mapping of Thick Oil Spills Using Imaging Spectroscopy." Open file Report 2010-1167.

Cloutis, E. A. 1989. "Spectral reflectance properties of hydrocarbons: remote-sensing implications." Science 245 (4914):165-8. doi: 10.1126/science.245.4914.165.

Correa Pabón, Rosa Elvira, and Carlos Roberto de Souza Filho. 2016. "Spectroscopic characterization of red latosols contaminated by petroleum-hydrocarbon and empirical model to estimate pollutant content and type." Remote Sensing of Environment 175 (Supplement C):323-336. doi: https://doi.org/10.1016/j.rse.2016.01.005.

Estes, John E., and Leslie W. Senger. 1971. "The multispectral concept as applied to marine oil spills." Remote Sensing of Environment 2:141-163. doi: http://dx.doi.org/10.1016/0034-4257(71)90088-5.

Etkin, Dagmar Schmidt. 2001. "Analysis of oil spill trends in the United States and worldwide." International Oil Spill Conference.

Fingas, M., and C. E. Brown. 2017. "Chapter 5 - Oil Spill Remote Sensing." In Oil Spill Science and Technology (Second Edition), 305-385. Boston: Gulf Professional Publishing.

Fingas, Mervin. 2016. Oil spill science and technology: Gulf professional publishing.

Fritt-Rasmussen, Janne, and Per Johan Brandvik. 2011. "Measuring ignitability for in situ burning of oil spills weathered under Arctic conditions: From laboratory studies to large-scale field experiments." Marine Pollution Bulletin 62 (8):1780-1785. doi: https://doi.org/10.1016/j.marpolbul.2011.05.020.

Fritt-Rasmussen, Janne, Per Johan Brandvik, Arne Villumsen, and Erling H. Stenby. 2012. "Comparing ignitability for in situ burning of oil spills for an asphaltenic, a waxy and a light crude oil as a function of weathering conditions under arctic conditions."

Cold Regions Science and Technology 72 (Supplement C):1-6. doi: https://doi.org/10.1016/j.coldregions.2011.12.001.

Hörig, B., F. Kühn, F. Oschütz, and F. Lehmann. 2001. "HyMap hyperspectral remote sensing to detect hydrocarbons." International Journal of Remote Sensing 22 (8):1413-1422. doi: 10.1080/01431160120909.

Kaufman, Yoram J, Andrew E Wald, Lorraine A Remer, Bo-Cai Gao, Rong-Rong Li, and Luke Flynn. 1997. "The MODIS 2.1-/spl mu/m channel-correlation with visible reflectance for use in remote sensing of aerosol." IEEE transactions on Geoscience and Remote Sensing 35 (5):1286-1298.

Kühn, F, K. Oppermann, and B. Hörig. 2004a. "Hydrocarbon Index – an algorithm for hyperspectral detection of hydrocarbons." International Journal of Remote Sensing 25 (12):2467-2473. doi: 10.1080/01431160310001642287.

Kühn, F, Konstanze Oppermann, and Bernhard Hörig. 2004b. "Hydrocarbon Index–an algorithm for hyperspectral detection of hydrocarbons." International Journal of Remote Sensing 25 (12):2467-2473.

Kvenvolden, KA, and CK Cooper. 2003. "Natural seepage of crude oil into the marine environment." Geo-Marine Letters 23 (3-4):140-146.

Lammoglia, T, and Carlos Roberto Souza Filho. 2012. "Satellite determination of API Gravity and Sara Components of Offshore Petroleum seeps." Revista Brasileira de Geofísica 4 (30):419-430.

Lammoglia, Talita, and Carlos Roberto de Souza Filho. 2011. "Spectroscopic characterization of oils yielded from Brazilian offshore basins: Potential applications of remote sensing." Remote Sensing of Environment 115 (10):2525-2535. doi: http://dx.doi.org/10.1016/j.rse.2011.04.038.

Lammoglia, Talita, and Carlos Roberto de Souza Filho. 2015. "Chronology and backtracking of oil slick trajectory to source in offshore environments using ultraspectral to multispectral remotely sensed data." International Journal of Applied Earth Observation and Geoinformation 39:113-119. doi: http://dx.doi.org/10.1016/j.jag.2015.03.007.

Lammoglia, Talita, and Carlos Roberto de Souza Filho. 2012a. "Mapping and characterization of the API gravity of offshore hydrocarbon seepages using multispectral ASTER data." Remote Sensing of Environment 123:381-389. doi: http://dx.doi.org/10.1016/j.rse.2012.03.026.

Lammoglia, Talita, and Carlos Roberto de Souza Filho. 2012b. "Mapping and characterization of the API gravity of offshore hydrocarbon seepages using multispectral ASTER data." Remote Sensing of Environment 123 (Supplement C):381-389. doi: https://doi.org/10.1016/j.rse.2012.03.026.

Leacock, Elspeth. 2005. The Exxon Valdez Oil Spill. Edited by Matt Levine. New York, United States of America: Facts On File, Inc.

Li, Pu, Qinhong Cai, Weiyun Lin, Bing Chen, and Baiyu Zhang. 2016. "Offshore oil spill response practices and emerging challenges." Marine Pollution Bulletin 110 (1):6-27. doi: https://doi.org/10.1016/j.marpolbul.2016.06.020.

Liu, Yao-Zhong, Astrid M. Roy-Engel, Melody C. Baddoo, Erik K. Flemington, Guangdi Wang, and He Wang. 2016. "The impact of oil spill to lung health—Insights from

an RNA-seq study of human airway epithelial cells." Gene 578 (1):38-51. doi: https://doi.org/10.1016/j.gene.2015.12.016.

Lu, Yingcheng, Wenfeng Zhan, and Chuanmin Hu. 2016. "Detecting and quantifying oil slick thickness by thermal remote sensing: A ground-based experiment." Remote Sensing of Environment 181:207-217. doi: http://dx.doi.org/10.1016/j.rse.2016.04.007.

Murphy, David, Brad Gemmell, Liana Vaccari, Cheng Li, Hernando Bacosa, Meredith Evans, Colbi Gemmell, Tracy Harvey, Maryam Jalali, and Tagbo H. R. Niepa. 2016. "An in-depth survey of the oil spill literature since 1968: Long term trends and changes since Deepwater Horizon." Marine Pollution Bulletin 113 (1):371-379. doi: https://doi.org/10.1016/j.marpolbul.2016.10.028.

National Research Council. 2003. Oil in the sea III: inputs, fates, and effects, Committee on Oil in the Sea: Inputs, Fates, and Effects Ocean Studies Board and Marine Board Divisions of Earth and Life Studies and Transportation Research Board. Washington, D.C.: National Academies Press.

Obida, Christopher B., G. Alan Blackburn, J. Duncan Whyatt, and Kirk T. Semple. 2018. "Quantifying the exposure of humans and the environment to oil pollution in the Niger Delta using advanced geostatistical techniques." Environment International 111 (Supplement C):32-42. doi: https://doi.org/10.1016/j.envint.2017.11.009

Olagunju K.T., Allen C. S., Olobaniyi S.B., Oyedele K.F (2023)."Hydrocarbon Spectra Slope (HYSS): A Spectra Index for Quantifying and Characterizing Hydrocarbon oil on Different Substrates Using Spectra Data." Journal of Geoscience, Engineering, Environment and Technology Vol. 08 No 2. Doi: https://doi.org/10.25299/jgeet.2023.8.2.9741

Richards, John A, and JA Richards. 1999. Remote sensing digital image analysis. Vol. 3: Springer.

Sarbatly, Rosalam, Duduku Krishnaiah, and Zykamilia Kamin. 2016. "A review of polymer nanofibres by electrospinning and their application in oil–water separation for cleaning up marine oil spills." Marine Pollution Bulletin 106 (1):8-16. doi: https://doi.org/10.1016/j.marpolbul.2016.03.037.

Scafutto, Rebecca Del'Papa Moreira, and Carlos Roberto de Souza Filho. 2016. "Quantitative characterization of crude oils and fuels in mineral substrates using reflectance spectroscopy: Implications for remote sensing." International Journal of Applied Earth Observation and Geoinformation 50 (Supplement):221-242. doi:

https://doi.org/10.1016/j.jag.2016.03.017.

Shi, X., P. W. Bellino, A. Simeoni, and A. S. Rangwala. 2016. "Experimental study of burning behavior of large-scale crude oil fires in ice cavities." Fire Safety Journal 79 (Supplement C):91-99. doi: https://doi.org/10.1016/j.firesaf.2015.11.007.

Sun, S., C. Hu, L. Feng, G. A. Swayze, J. Holmes, G. Graettinger, I. MacDonald, O. Garcia, and I. Leifer. 2016. "Oil slick morphology derived from AVIRIS measurements of the Deepwater Horizon oil spill: Implications for spatial resolution requirements of remote sensors." Mar Pollut Bull 103 (1-2):276-85. doi: 10.1016/j.marpolbul.2015.12.003.

Svejkovsky, J, and J Muskat. 2006. "Real-time detection of oil slick thickness patterns with a portable multispectral sensor." US Department of the Interior Minerals Management Service.

Svejkovsky, Jan, Mark Hess, Judd Muskat, Tim J. Nedwed, Jenifer McCall, and Oscar Garcia. 2016. "Characterization of surface oil thickness distribution patterns observed during the Deepwater Horizon (MC-252) oil spill with aerial and satellite remote sensing." Marine Pollution Bulletin 110 (1):162-176. doi:

https://doi.org/10.1016/j.marpolbul.2016.06.066.

Tatem, H. E., B. A. Cox, and J. W. Anderson. 1978. "The toxicity of oils and petroleum hydrocarbons to estuarine crustaceans." Estuarine and Coastal Marine Science 6 (4):365-373. doi: https://doi.org/10.1016/0302-3524(78)90128-7.

Tou, JT, and RC Gonzalez. 1974. "Pattern Recognition Principles Addison-Wesley." Reading, MA 377.

Waldichuk, Michael. 1974. "Coastal marine pollution and fish." Ocean Management 2 (1):1-60. doi: https://doi.org/10.1016/0302-184X(74)90009-2.

Wettle, Magnus, Paul J. Daniel, Graham A. Logan, and Medhavy Thankappan. 2009. "Assessing the effect of hydrocarbon oil type and thickness on a remote sensing signal: A sensitivity study based on the optical properties of two different oil types and the HYMAP and Quickbird sensors." Remote Sensing of Environment 113 (9):2000-010. doi: https://doi.org/10.1016/j.rse.2009.05.010.

Zhenghao Shi and Ko B. Fung. 1994. "A Comparison of Digital Speckle Filters " Proceedings of IGARSS 94 August 8-12:2129-2133.